Shock-induced collapse of bubbles in liquid

X. Y. Hu and N. A. Adams

Lehrstuhl für Aerodynamik, Technische Universität München, 85748 Garching, Germany

Summary. The problem of shock-induced collapse of bubbles in liquid is investigated for 3 types of bubble configuration (bubble row, bubble cluster and bubble matrix) by numerical simulations with a newly developed conservative multi-phase method. The computational results show complex processes which are strongly influenced by the interactions between shock waves, liquid jets, sound waves, vortex sheets and vortices, and bubble oscillations (collapse and rebounce). Some observations and predictions from previous studies are also verified.

1 Introduction

Understanding the high-speed dynamics of bubbles in liquid is important both for fundamental research and applications. The high-speed dynamical phenomena usually are introduced by the collapse of bubbles under certain ambient condition. When a bubble is under shock impact, it begins an asymmetric collapse which is characterized by producing a high-speed liquid jet. The collapse of a single bubble is understood quite well by means of experiments [2] and numerical simulations [3][4]. However, for the collapse evolving multiple bubbles, while experimental studies were carried almost 20 years ago [1], detailed numerical simulation has not been done for serious difficulties on interface modeling. Recently, we developed a conservative interface method for multi-phase problems [5], which solves the difficulty of conservation for the front tracking method and treats the topological changes naturally by combining interface description and geometric operations with a level set technique. In this paper, we present the simulations with the new method on the collapse of bubbles for 3 types of configuration: bubble row, bubble cluster and bubble matrix.

2 Numerical models

We model the flows of water and air with compressible Eulerian equations in two spatial dimensions, that is

$$\frac{\partial \mathbf{U}}{\partial t} + \frac{\partial \mathbf{F}(\mathbf{U})}{\partial x} + \frac{\partial \mathbf{G}(\mathbf{U})}{\partial y}, \tag{1}$$

where

$$\mathbf{U} = \begin{pmatrix} \rho \\ \rho u \\ \rho v \\ E \end{pmatrix}, \mathbf{F}(\mathbf{U}) = \begin{pmatrix} \rho u \\ \rho u^2 + p \\ \rho uv \\ (E+p)u \end{pmatrix}, \mathbf{G}(\mathbf{U}) = \begin{pmatrix} \rho v \\ \rho uv \\ \rho v^2 + p \\ (E+p)v \end{pmatrix},$$

in which the total energy density $E = \rho e + \frac{\rho(u^2+v^2)}{2}$, e is the internal energy per unit mass. To close this set of equations, the pressure is obtained by the equation of states, which

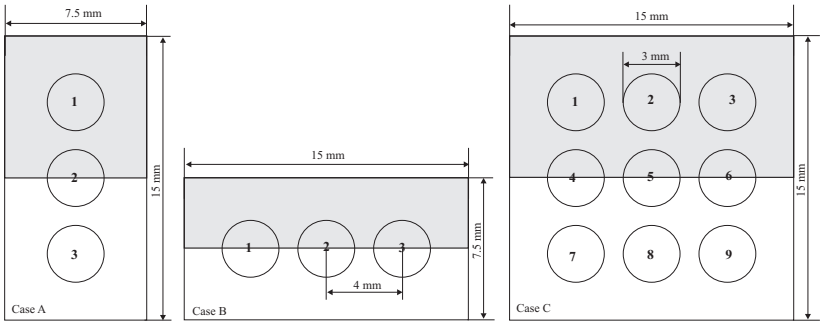

Fig. 1. Schematic for the computational setups for the three cases, in which the computational domains are the dark regions.

is given as Tait's equation for water $p = B\left(\frac{\rho}{\rho_o}\right)^{\gamma} - B + A$ where $\gamma = 7.15$, $A = 10^5$Pa, $B = 3.31 \times 10^8$Pa, and $\rho_o = 1000kg/m^3$, and the idea gas equation for air $p = (\gamma - 1)\rho e$ where $\gamma = 1.4$. At present, no cavitation model is included for water. The evolution of water/air interface is given by the level set equation

$$\frac{\partial \phi}{\partial t} + u\frac{\partial \phi}{\partial x} + v\frac{\partial \phi}{\partial y} \tag{2}$$

in which water is defined in the sub-domain with $\phi > 0$ and air in the sub-domain with $\phi < 0$.

3 Results

In this work, three cases are studied, in which, (Case A) a vertical row of 3 bubbles, (Case B) a horizontal cluster of 3 bubbles and (Case C) a matrix of 9 bubbles are embedded in rectangular or square domains. The schematic for the computational setups are shown in Fig. 1. In all the cases, a planar shock wave with the shock pressure of 0.26 GPa from the left, which is about the same strength as that in the experiment [1], and circular, two-dimensional air bubbles (diameter 3 mm and 4 mm apart) are used. Since a symmetric condition is used for the lower boundary, only the upper half of the domain is computed. An supersonic in-flow condition is used for the left boundary, and an out-flow condition with zero gradient is applied to both the right and the upper boundaries. A gird size of 1.875×10^{-5} mm, and a CFL number of 0.6 are used in all the computations.

Case A Figure 2 shows the density gradients at 4 time instances after the shock wave impinges the bubbles. At the early stage, as shown in Fig. 2a, it is observed that the wave structure comprises the two incident shocks I_1 and I_2 which is weaker for the stronger rarefaction from the two bubble surfaces, the reflection waves R_1 and R_2 which is reflected back and forth from the bubble surfaces to form secondary reflection waves R_2', and the transmitted shocks T inside the bubbles. It is also observed that there are weak sound waves S_1 near the bubble surface, especially the segments with larger curvatures, as shown in Fig. 2b. For bubble 1, because of the asymmetric rarefaction and reflection, the collapse velocity of the upper surface is larger than that of the lower surface. Consequentially, the liquid jet J_1 collides the bubble surface asymmetrically

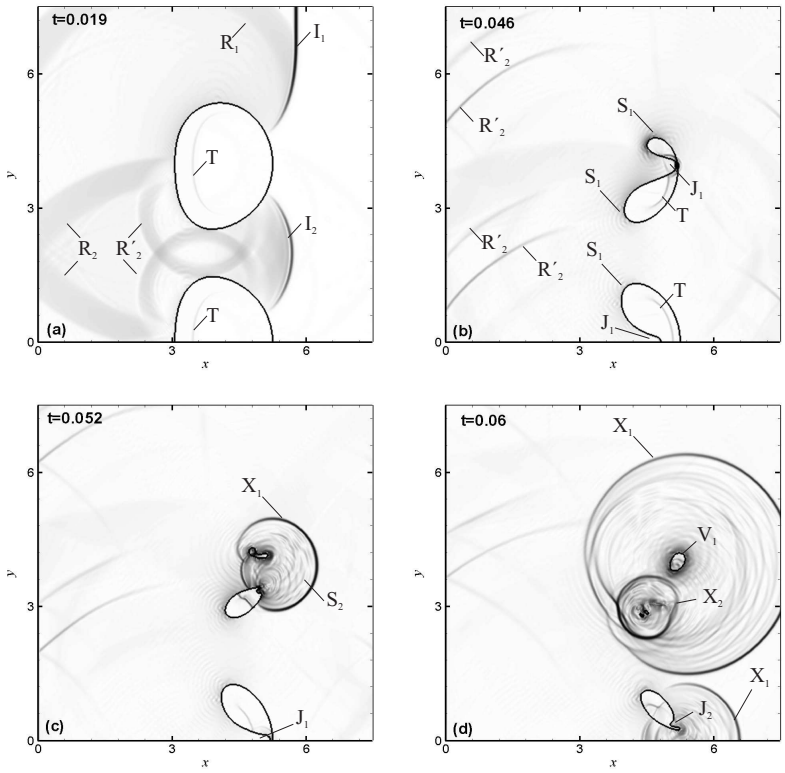

Fig. 2. Case A: Density gradients at 3 time instances.

with the speed about 900 m/s (more than twice of the measured value in experiments [1]) and earlier than bubble 2, as shown in Fig. 2b. Note that, before the collision, the transmitted shock wave has been reflected from the bubble surface and collided with the liquid jet. After the collision, a strong explosion wave X_1 is produced and the bubble is split into two bubbles with different sizes. The smaller one quickly comes to its minimum volume, as shown in Fig.2c, and begins to re-bounce and rotate in anti-clockwise, by which sound waves S_2 much stronger than S_1 are produced after X_1. As the present air/water interface is treated as inviscid, sharp density discontinuity, the rotating bubble is actually a closed vortex sheet V_1. On the other hand, the larger one goes for secondary collapse which leads to a secondary explosion wave X_2, as shown in Fig. 2d, with a shock pressure much higher than that of X_1. This result suggests that the secondary collapse is more mechanically destructive than the liquid-jet collision [6]. Comparing to bubble 1, a symmetric but weaker jet J_1 with the speed about 700 m/s leads to a weaker explosion wave and a secondary jet J_2, which will split the upper half of the bubble further.

Case B For bubble 1, after the liquid jet J_1 collides with the bubble surface with the speed about 1100 m/s and produces an explosion wave X_1. The upper half of the bubble forms a new bubble which quickly comes to its minimum volume and begins to re-bounce, companying with several weak explosion waves W_1 and sound waves S_2, as shown in Fig. 3a. The re-bouncing bubble rotates in anti-clockwise and forms a closed vortex sheet V_1.

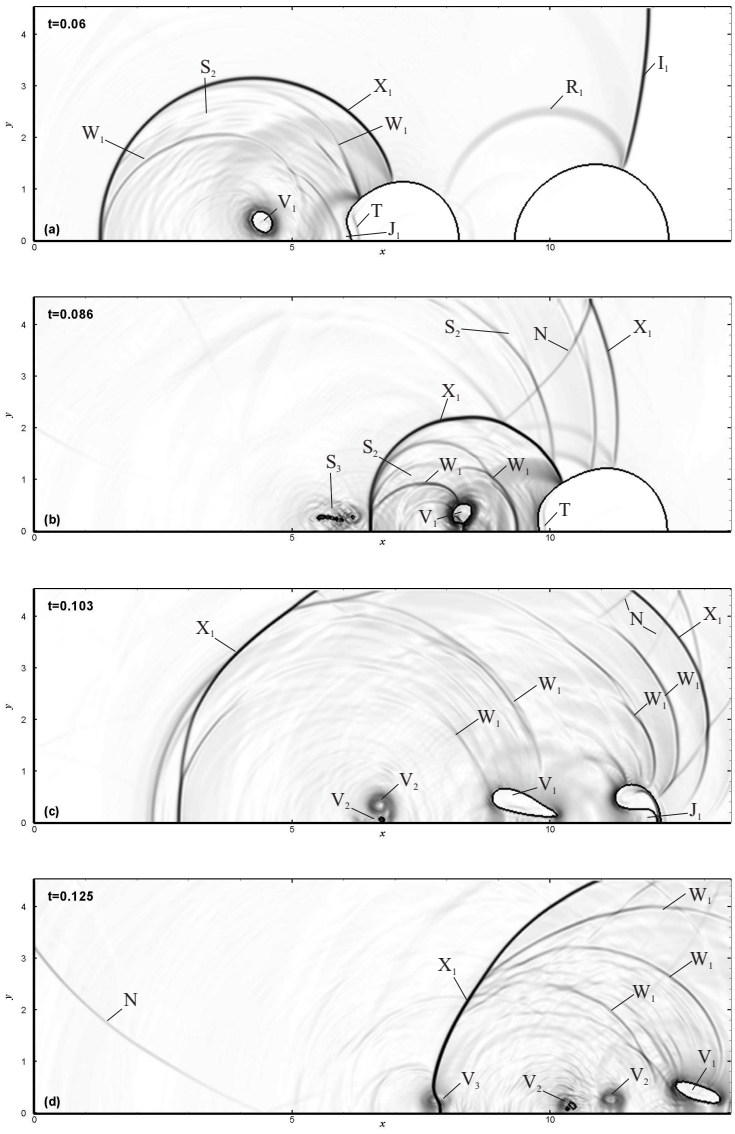

Fig. 3. Case B: Density gradients at 4 time instances.

The vortex sheet is stretched greatly and generates sound waves S_3, as shown in Fig. 3b. Under the compression of the explosion wave from bubble 2, as shown in Fig. 3c, the vortex sheets collapses finally, by which most of the air mass are split to unresolved bubbles (air mass is deleted in the present model) and only the two tip vortices V_2 are survived. As the tip vortices are attracted to each other, they approach gradually and merge to a single vortex V_3, as shown in Fig. 3d. During the merging process, the last part of air mass is also collapsed into unresolved bubbles. The merged vortex then is impact by the explosion wave originated from bubble 3, which produces weak

compression waves because of the shock/vortex interaction. Note that there are some weak reflection wave fronts N originating from the boundary. These waves are artifacts caused by the simple out-flow boundary condition and have no considerable influence to the global collapse process. Comparing to bubble 1, the behaviors of bubble 2 and bubble 3 are quite similar. The difference is that the explosion waves produced by previously impacted bubbles increase the size and the speed of the liquid jet, as shown in Fig. 3c. The speed of the liquid jet J_1 in bubble 2 is about 1500 m/s and in bubble 3 is about 1600 m/s. On the other hand, if more than 3 bubbles are considered in this case, eventually, the same collapse process will repeat until the end of the bubble cluster. However, as only three bubbles are considered in this case, there is no process after the merge of the tip vortices for bubble 2 and no process after the collapse of the vortex sheets for bubble 3.

Case C In this case, the early stage is quite close to the entire process of Case A. As shown in Fig. 4a, an asymmetric liquid jet with the speed about 900 m/s is produced in bubble 1, which split the bubble into two bubbles with different sizes. While the smaller one quickly goes to re-bounce and forms a vortex sheet V_1, the larger one continues collapse and produces a secondary explosion wave X_2. During the collapse, the bubble is split into 3 tiny bubbles and a strong clockwise vortex V_2 is formed. Comparable weak liquid jet with the speed about 700 m/s is produced in bubble 4, which again produces a weaker explosion wave X_1. The secondary jet in bubble 4 then splits the upper half part of the bubble into two bubbles. By the compression of the explosion waves from bubble 1, these split bubbles collapse and produces a secondary explosion wave X_2 for the larger bubble and a weak explosion wave W_2 for the smaller bubble, which is further split into unresolved bubble, and left an anti-clockwise vortex V_2, as shown in Fig. 4b. After being compressed by the reflected explosion wave Rx_2, the larger bubble collapse again and produces another weak explosion wave W_3. The tiny bubbles and the vortex left from bubble 1 is also compressed by the explosion wave from bubble 4 and the reflected explosion waves. While the collapse and re-bouncing of the tiny bubbles produce several sound waves S_3, the vortex/shock interaction produces two weak explosion waves W_4, as shown in Fig. 4c. Comparing to bubble 1, the liquid jet in bubble 2 is also asymmetric, but with larger size and higher speed (about 1100 m/s). Similarly, the liquid jet produced in bubble 5 has also larger size and higher speed (about 1000 m/s) than that of bubble 4.

4 Conclusion

We have studied the problem of shock-induced collapse of bubbles in liquid by numerical simulations. The results suggest that: (a) the calculated liquid jet speeds are much larger than those measured in experiments; (b) after the first liquid-jet impact, the split bubble may re-bounce quickly or develop to secondary collapse, and the highest pressure happens after the secondary collapse; (c) there are complex interactions between shock waves, vortex sheets or vortices; (d) with the present computational setups, the multiple-bubble collapse increase the size and speed of liquid jets.

References

1. Dear JP and Field JE: J Fluid Mech **190** (1988)

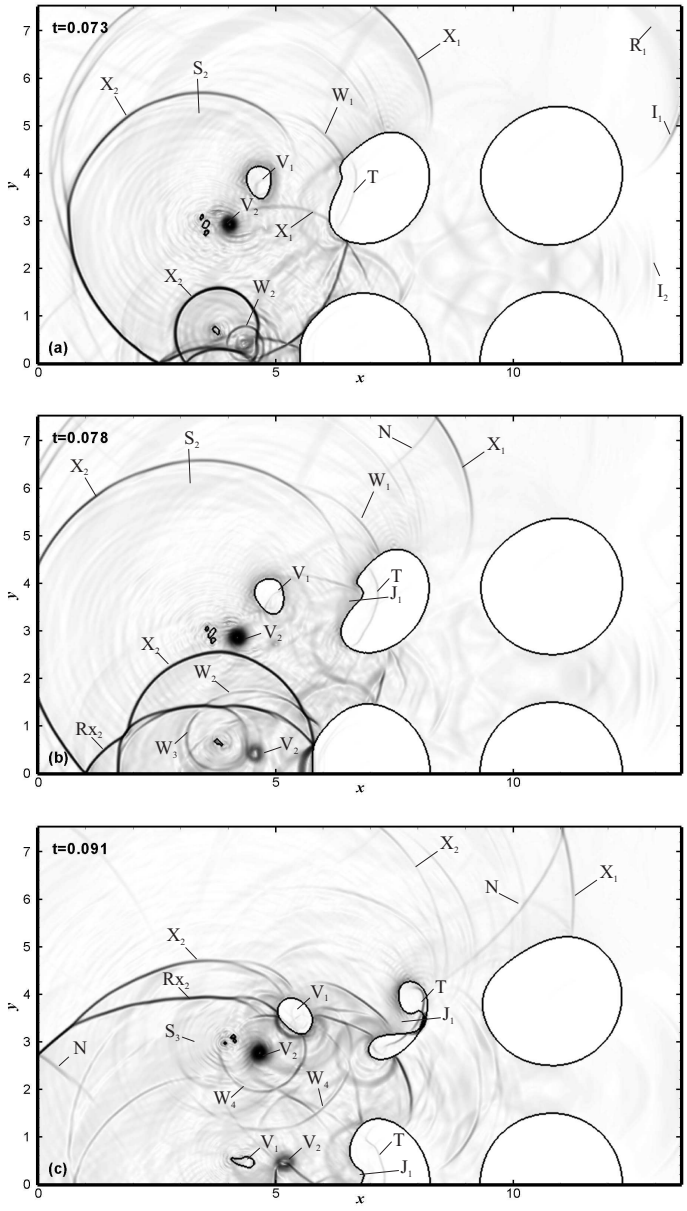

Fig. 4. Case C: Density gradients at 4 time instances.

2. Bourne NK and Field JE: J Fluid Mech **244** (1992)
3. Ball GJ, Howell BP, Leighton TG, Schofield MJ: Shock Waves **10** 4 (2000)
4. Hu XY and Khoo BC: J Comput Phys **198** 1 (2004)
5. Hu XY, Khoo BC, Adams NA, Huang FL: J Comput Phys **219** 2 (2006)
6. Philipp A and Lauterborn W: J Fluid Mech **361** (1998)